AIP | Applied Physics Letters

Soft x-ray ptychography studies of nanoscale magnetic and structural correlations in thin SmCo5 films

X. Shi, P. Fischer, V. Neu, D. Elefant, J. C. T. Lee, D. A. Shapiro, M. Farmand, T. Tyliszczak, H.-W. Shiu, S. Marchesini, S. Roy, and S. D. Kevan

Citation: Applied Physics Letters **108**, 094103 (2016); doi: 10.1063/1.4942776
View online: http://dx.doi.org/10.1063/1.4942776
View Table of Contents: http://scitation.aip.org/content/aip/journal/apl/108/9?ver=pdfcov
Published by the AIP Publishing

Soft x-ray ptychography studies of nanoscale magnetic and structural correlations in thin $SmCo_5$ films

X. Shi,[1,2] P. Fischer,[3,4] V. Neu,[5] D. Elefant,[5] J. C. T. Lee,[1,2,3] D. A. Shapiro,[1] M. Farmand,[1] T. Tyliszczak,[1] H.-W. Shiu,[1,6] S. Marchesini,[1] S. Roy,[1] and S. D. Kevan[1,2,3,a)]
[1]*Advanced Light Source, Lawrence Berkeley National Laboratory, Berkeley, California 94720, USA*
[2]*Department of Physics, University of Oregon, Eugene, Oregon 97401, USA*
[3]*Materials Sciences Division, Lawrence Berkeley National Laboratory, Berkeley, California 94720, USA*
[4]*Department of Physics, University of California, Santa Cruz, California 94056, USA*
[5]*IFW Dresden, Institute for Metallic Materials, Helmholtzstr. 20, D-01069 Dresden, Germany*
[6]*National Synchrotron Radiation Research Center (NSRRC), 101 Hsin-Ann Road, Hsinchu Science Park, Hsinchu 30076, Taiwan*

(Received 2 December 2015; accepted 12 February 2016; published online 2 March 2016)

High spatial resolution magnetic x-ray spectromicroscopy at x-ray photon energies near the cobalt L_3 resonance was applied to probe an amorphous 50 nm thin $SmCo_5$ film prepared by off-axis pulsed laser deposition onto an x-ray transparent 200 nm thin Si_3N_4 membrane. Alternating gradient magnetometry shows a strong in-plane anisotropy and an only weak perpendicular magnetic anisotropy, which is confirmed by magnetic transmission soft x-ray microscopy images showing over a field of view of 10 μm a primarily stripe-like domain pattern but with local labyrinth-like domains. Soft x-ray ptychography in amplitude and phase contrast was used to identify and characterize local magnetic and structural features over a field of view of 1 μm with a spatial resolution of about 10 nm. There, the magnetic labyrinth domain patterns are accompanied by nanoscale structural inclusions that are primarily located in close proximity to the magnetic domain walls. Our analysis suggests that these inclusions are nanocrystalline Sm_2Co_{17} phases with nominally in-plane magnetic anisotropy. © *2016 AIP Publishing LLC*. [http://dx.doi.org/10.1063/1.4942776]

Understanding and controlling the spatial correlations between magnetic and structural heterogeneity lies at the heart of diverse magnetic technologies that find wide ranging applications, from power generation, transmission, and conversion to nanoscale magnetic devices in sensor and information technologies.[1–4] These correlations are of particular interest for non-collinear spin configurations in magnetic materials, which are proposed for emerging low power information processing technologies.[5,6] Such spin textures conventionally occur at the boundary between magnetic domains, but are also important at magnetic interfaces, near magnetic nanostructures, and in topological textures like skyrmions. To understand these textures at relevant length scales will require developing and deploying microscopy techniques that offer sub-10 nm spatial resolution in three dimensions combined with high sensitivity to vector magnetization.[7]

X-ray magnetic microscopies, including x-ray photoemission electron microscopy (X-PEEM), x-ray holography (XRH), and Fresnel zone plate (FZP) based full field and scanning x-ray techniques (MTXM and STXM), have been developed over the past two decades.[8,9] In coherent diffraction imaging (CDI)[10] and ptychography,[11–13] speckle-diffraction patterns are recorded with high numerical aperture detectors, and phase retrieval algorithms[14,15] are used to recover real space phase and amplitude images at a spatial resolution well below the incident x-ray spot size (about 50–70 nm). Soft x-ray ptychography has recently achieved 3 nm resolution on high-contrast non-magnetic test objects[13] and 10 nm resolution on heterogeneous micron-sized particles with chemical sensitivity.[16]

Magnetic soft x-ray microscopies, specifically X-PEEM[17] and MTXM,[18] offer the requisite sensitivities for 3D magnetic imaging, but studies to date have achieved typically only 20–25 nm resolution, which is not sufficient to probe characteristic spatial scales of magnetic inhomogeneities in many systems.[19]

Here, we report the application of resonant soft x-ray ptychography, an emerging, robust variant of x-ray CDI,[10] to probe an amorphous $SmCo_5$ thin film that exhibits perpendicular magnetic anisotropy (PMA).[20] We combined polarization-dependent ptychography with dichroic scattering contrast near the Co L_3 absorption edge to produce high-resolution phase and amplitude images with element-specific contrast to distinguish magnetic and structural textures. Applying a Fourier Ring Correlation (FRC) analysis to estimate both the structural and magnetic resolution, we find both to be ~10 nm. Using this emerging magnetic imaging technique, we measure the magnetic domain labyrinth in the $SmCo_5$ film and observe a correlation between nanoscale structural inclusions and the magnetic domain structure. Polarized x-ray absorption spectroscopy suggests that these inclusions are nanocrystalline Sm_2Co_{17} phases with nominally in-plane magnetic anisotropy.

The 50 nm thick $SmCo_5$ film sample used in this study was grown by off-axis pulsed laser deposition (PLD) in 0.1 mbar Ar background pressure onto a heated x-ray transparent 200 nm thick Si_3N_4 membrane ($T_{substrate} = 400\,^{\circ}C$). The $SmCo_5$ layer was sandwiched between a 7 nm thin Cr buffer and cover layers for oxygen protection. While

a)Author to whom correspondence should be addressed. Electronic mail: SDKevan@lbl.gov

similarly prepared PLD $SmCo_5$ films deposited under UHV conditions crystallize directly upon deposition on a heated Si_3N_4/Si substrate and develop a preferred in-plane texture (c-axis in the film plane),[21,22] these films remain x-ray amorphous due to the lower kinetic energy of the material plasma and obtain a perpendicular magnetic anisotropy.

Alternating gradient magnetization loops shown in Fig. 1(a) indicate a pronounced in-plane anisotropy with a much weaker PMA. Whereas the former leads to a dominant stripe domain pattern, a strong PMA yields a labyrinth domain pattern. Magnetic transmission soft x-ray microscopy (Fig. 1(b)) covering a field of view of several μm with a spatial resolution of about 25 nm shows indeed a magnetic domain structure that resembles both, a primarily stripe-like domain pattern, that locally vary towards a more labyrinth-like domain structure.

To obtain further insight into the local spin structure, ptychographic imaging was performed using the experimental setup described previously[13] and located at beamline 11.0.2 of the Advanced Light Source, as shown schematically in Fig. 1(c). All results presented here were recorded in zero magnetic field with the film in the as-prepared demagnetized state and at ambient temperature. A monochromatized, transversely coherent, and circularly polarized soft x-ray beam with ~90% degree of polarization tuned near the Co L_3 edge at 778.6 eV was focused using an FZP lens at normal incidence onto the $SmCo_5$ film. The FZP had a 60 nm outer zone width and provided an approximately 75 nm focal spot on the sample. Diffraction patterns were collected in a transmission geometry using a 1300×1340 pixel charge coupled device (CCD) detector placed 60 mm downstream of the sample. Ptychography scans consisted of collecting 20×20 diffraction patterns at 50 nm spacing in orthogonal directions. Two diffraction patterns with 10 ms and 400 ms exposure times were collected at each scan point to measure regions of higher signal at low momentum transfer and lower signal at high momentum transfer, respectively. These were combined to extend the dynamic range of the measurements, thereby improving the spatial resolution.[13]

A typical diffraction pattern is shown in Fig. 1(d). The intensity profile is not radially symmetric, which is again indicative of a non-symmetric component to the scattering textures. To modulate the magnetic contrast (X-ray magnetic circular dichroism, XMCD) at each scan point, independent measurements were performed using left and right circular polarization. This enabled to distinguish magnetic and charge textures by combining those polarization dependent phase and amplitude images. Finally, measurements were performed at three photon energies, specifically at 778.0 eV just below the L_3 absorption edge to provide dominant (magnetic) phase contrast, at the absorption maximum at 778.6 eV to provide dominant (magnetic) absorption contrast, and above the main absorption white line at 780 eV, where the imaginary part of the refractive index δ has crossed zero to provide inverted magnetic phase contrast.[23,24] Ptychographic reconstructions of phase and amplitude images were performed using 300 iterations of the standard methods in the SHARP ptychography package.[25,26] The values of the resonant contribution to the real and imaginary parts of the refractive index derived from our ptychographic analysis at the three photon energies are in very good agreement with those derived from holographic imaging with better spectral sampling though with poorer spatial resolution.[24]

Figs. 2(a)–2(f) show the reconstructed amplitude and phase images collected at the three photon energies all with left circular polarization. Figs. 2(e) and 2(f) are different sample positions than (a)–(d), and the inversion in phase contrast noted above is readily apparent by noting that the amplitude and phase contrast are the same above the edge but opposite below the edge. The $SmCo_5$ magnetic domains exhibit a labyrinthine structure as expected for a PMA film, with an average domain width of 76.5 nm. The domain

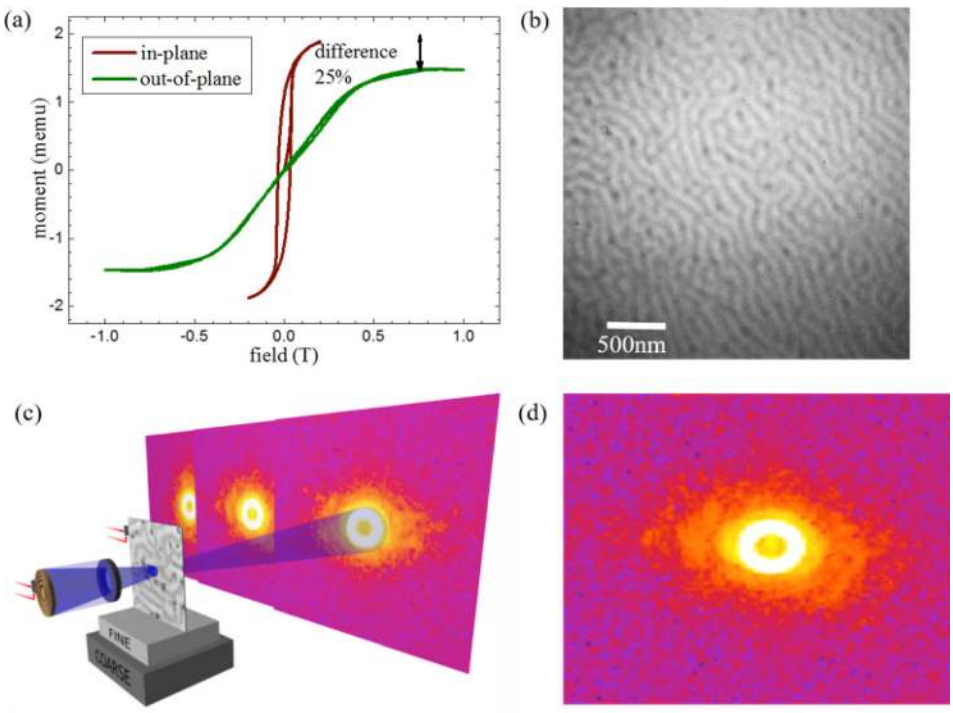

FIG. 1. (a) Magnetic hysteresis loop of the $SmCo_5$ film for in-plane and out-of-plane contributions. (b) Magnetic transmission soft x-ray microscopy image taken at BL 6.1.2 at the Advanced Light Source in Berkeley showing stripe-like domains with local distortions into labyrinth domains as well as dark inclusions. (c) Schematics of the ptychography setup at beamline 11.0.2 at the STXM branch at the Advanced Light Source. A Fresnel-Zone-Plate (FZP) focuses the x-ray beam through an order-sorting-aperture (OSA) onto the $SmCo_5$ thin film sample. Coherent diffraction patterns are collected on a charge coupled device detector. (d) Example of a single diffraction pattern showing experimental data of $SmCo_5$ sample.

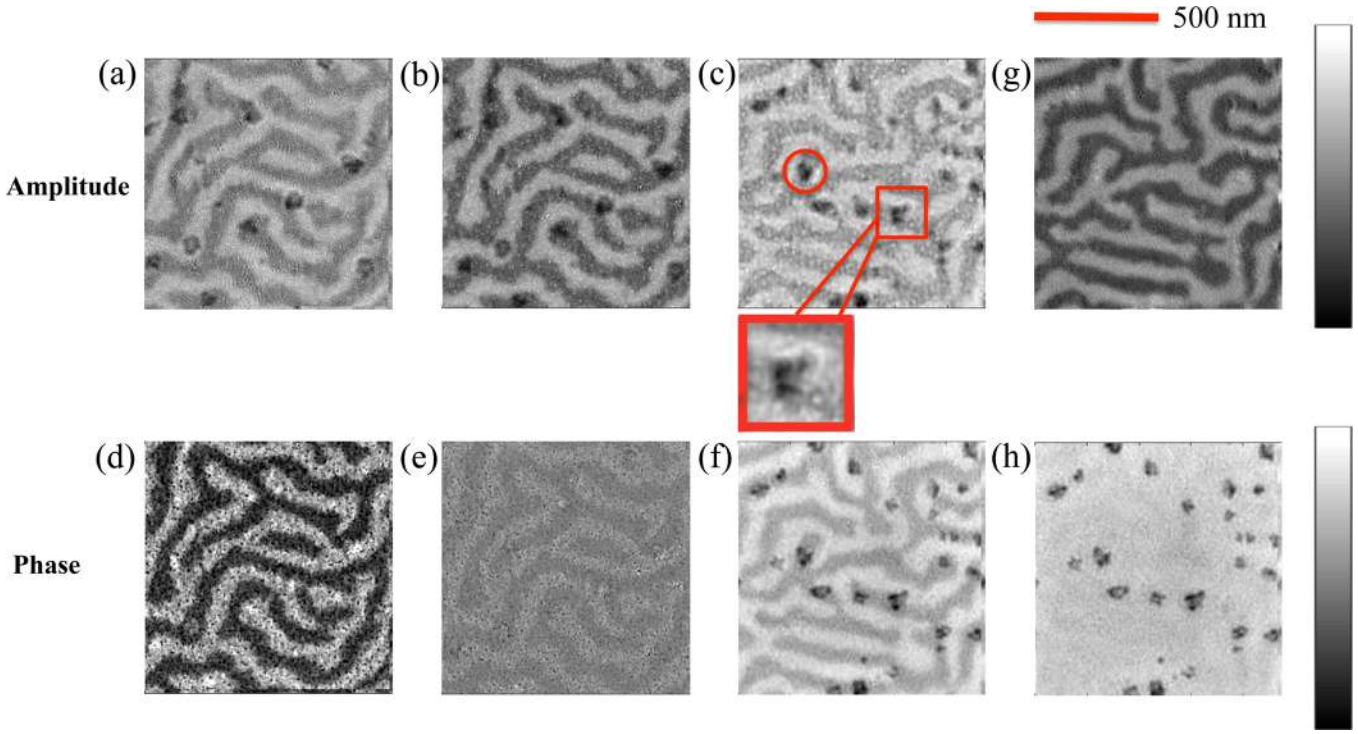

FIG. 2. Reconstructed amplitude (a)–(c) and phase (d)–(f) components of three x-ray energies of $SmCo_5$ thin film sample in transmission geometry. (a) and (d) are reconstructions at x-ray energy of 778 eV; (b) and (e) are reconstructions at x-ray energy of 778.6 eV; and (c) and (f) are reconstructions at x-ray energy of 780 eV. Red open circle and square (with red zoomed open square) indicate the inclusions present in the thin film sample. Note that in (d), the inclusions have opposite contrast (white color), indicating that the phase contrast is reversed compared to phase contrast in (f). The gray-scale bar is in the range of −0.2 to 0.5 rad. The phase component of the refractive index changes sign when going through the absorption component maximum. (g) Difference of left and right polarized reconstructed phase images at 780 eV x-ray energy taken at the position shown in (c) and (f). The gray-scale bar is in the range of −0.4 to 0.4 rad. (h) Sum of left and right polarized reconstructed phase images at 780 eV x-ray energy. The gray-scale bar is in the range of 0 to 1.2 rad.

patterns were reconstructed with high reproducibility from independent measurements. Fig. 2(g) shows the difference of right and left circular polarized phase images collected at 780 eV, i.e., above the resonant energy, where both amplitude and phase contrast are similar. As the XMCD contrast changes its sign with opposite polarization, this difference image isolates features with a component of magnetization along the photon propagation direction.[23,24] As expected for perpendicular magnetic anisotropy, the observed features are the domain labyrinth. The dark spots (="inclusions") apparent in the individual images in Figs. 2(a)–2(f) are mostly absent in the difference phase image. In contrast, Fig. 2(h) shows the sum of the same two phase images as in Fig. 2(g), which mimics an image collected with linear polarization where the signal is quadratic in magnetization and the magnetic contrast of the domain labyrinth should be small. The magnetic domains are indeed barely visible, while the scattering from the inclusions is enhanced. This suggests that the inclusions are dominated by charge scattering, though they may be ferromagnetic but with in-plane anisotropy which is not visible in the experimental geometry used here; we will return to this issue below. A powerful aspect of polarization-dependent soft x-ray microscopy is this straightforward separation of features associated with magnetic and charge scattering.

The spatial resolution achieved with ptychography is not determined purely by the numerical aperture of the detector because it depends crucially on the measured signal at high spatial frequency, which depends strongly on the sample's scattering contrast, as well as any systematic perturbations to the data, i.e., sample positioning errors, drift, or unstable illumination. This needs careful consideration specifically for magnetic systems, where the charge-scattered signal is significantly stronger than magnetic scattered signal,[27] and one might expect the corresponding resolutions to be different. To estimate our structural and magnetic resolution independently, we applied an FRC analysis[28] separately to the Fourier transforms of Figs. 2(g) and 2(h). The FRC measures the spatial frequency dependence of the cross-correlation of diffracted intensity from two independently measured and reconstructed datasets. In our case, we reconstructed "separate" images from a single ptychography scan using even- and odd-numbered 2D scan positions. This approach ensured perfect registry of the resulting images, but provided a conservative estimate of the true resolution because only half of the total available data were used in each image. The resulting FRC results are shown in Fig. 3; the spatial frequency where these curves cross a threshold is the estimated resolution. A slight shift to lower frequency for magnetic relative to charge scattering does indeed suggest that our resolution is slightly better for charge than magnetic features. That the shift is small is probably related to the fact that scattered intensity depends much more strongly on spatial frequency than sample contrast.[29] The reported numerical resolution depends on the criterion applied to the FRC curves; a threshold of 0.5 suggests charge and magnetic resolution of 12 and 10 nm, respectively, while the half-bit threshold places them both near 7 nm.

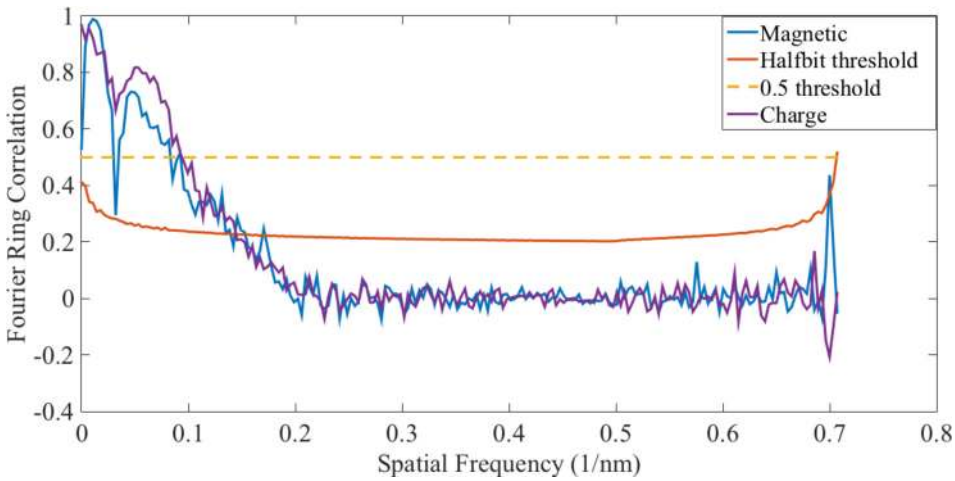

FIG. 3. (a) FRC resolution analysis. From the analysis, the 0.5 threshold determines a spatial resolution of 11 nm, the half-bit threshold determines the spatial resolution of 8 nm, and this is applied to both pure magnetic and pure charge reconstructed images displayed in Figs. 2(g) and 2(h).

Achieving this high spatial resolution offers the ability to estimate the domain wall (DW) width in this high anisotropy system. Measuring along cuts perpendicular to the DWs in Fig. 2(g), the convolution of our magnetic resolution with the actual DW width results to that the experimental DW width is on average about 15 nm. The width of a DW Δ can be calculated by $\Delta \approx \pi\sqrt{(A/K_U)}$, with A being the exchange constant and K_U the anisotropy constant. Δ can range from a few nanometers for hard magnets, such as $Nd_2Fe_{14}B$,[30] to tens of nanometers for soft magnetic materials, e.g., permalloy ($Fe_{20}Ni_{80}$)[30] or CoFe/Pd multilayers.[31] The in-plane and out-of-plane magnetization loops shown in Fig. 1(a) for the $SmCo_5$ thin film studied here allow J and K_U to be estimated and the actual domain wall width is predicted to be ~10 nm, in agreement with expectations given our spatial resolution.

The nature of the inclusions in Fig. 2 can be investigated in greater detail using the inherent spectroscopic sensitivity of x-ray microscopies, such as scanning transmission X-ray microscopy (STXM), full-field transmission X-ray microscopy, X-ray photoemission microscopy, or diffraction imaging based x-ray microscopies.[8] While the films are deposited with a nominal $SmCo_5$ composition, the equilibrium Sm-Co phase diagram is complex, and therefore crystalline compounds off the nominal film composition might nucleate during growth. Spectroscopic STXM measurements at the Co L edges show with a spatial resolution of about 20 nm systematically significant differences above and below the Co edge indicative of a chemical modification at those inclusions. A quantitative analysis of the ptychography images in Fig. 2 indicates ~23% and ~50% higher absorption on the inclusions than on the domain labyrinth at 778 eV and 780 eV, respectively. For comparison, the calculated non-resonant difference in absorption between crystalline $SmCo_5$ and Sm_2Co_{17} is ~19%,[32] which is comfortably close to the measured pre-edge difference at 778 eV. The composition of the inclusions is consistent with Sm_2Co_{17}, which is the lowest temperature congruently melting phase adjacent to the nominal film composition.

Many of the inclusions appear to have an internal structure, suggesting that the inclusions cluster after nucleation or, more likely, nearby nucleation events are spatially correlated, e.g., by stress in the film during growth. The smallest observed structures, either embedded in an inclusion or isolated, have a size of ~12 nm. Finally, several of the inclusions are partly bordered by a ring of apparently lower x-ray absorption and, therefore, of lower cobalt concentration; a good example is provided in the inset in Fig. 2(c). The width of these rings is near the limit of our spatial resolution and might also be artifacts of the ptychographic reconstruction. However, the rings are consistent with short-range diffusion from the $SmCo_5$ film to grow a nucleated, cobalt-rich nanocrystalline phase, e.g., Sm_2Co_{17}.

We now turn our attention to the interaction between magnetic and structural heterogeneities. In particular, we observe that the inclusions tend to avoid overlapping with a DW or vice versa, the DW is repelled from those inclusions. Interestingly, we found the DW to be in close proximity to the inclusions. This affinity between a DW and inclusion points to a spin canting and suggests that the inclusions might be magnetic but with in-plane magnetization. Such a configuration would be consistent with the lack of magnetic contrast for the inclusions observed in Fig. 2(g). A more careful examination of Fig. 2(g) indicates that some of these inclusions are faintly visible, suggesting that their magnetization vectors might be slightly canted into or out of film plane. Assuming that this is true, a complex spin structure would exist at the interface of these inclusions, though presently we lack the resolution to measure such features in detail. Of course, the possible deficit in cobalt concentration around the inclusions noted above might also provide a mechanism to pin domain walls. It is worth noting that a recent magnetic soft x-ray spectromicroscopy reported a reduced L_3/L_2 value at the DW in a (Co 0.3 nm/Pt 0.5 nm) × 30 multilayer film with pronounced PMA, which also indicates a more complex spin texture inside the DW.[33]

Collecting these ideas, a proposed explanation is that the inclusions are nanocrystalline Sm_2Co_{17} particles that nucleated during film growth and that have nearly in-plane magnetization. The presence of cobalt-rich nanocrystals then requires a surrounding region of lower cobalt concentration, reflecting the complexity of the reaction, diffusion, and nucleation processes involved in film growth. Further validation of a detailed model like this will benefit from higher resolution and 3D tomographic reconstructions, which is expected to become available in the future.

In conclusion, we have applied an emerging, high resolution soft x-ray microscopy technique to study the nanoscale

magnetic and structural properties of thin $SmCo_5$ films. Ptychography with circularly polarized x-rays retrieved both absorption and phase contrast images of the magnetic domain structure and structural inclusions in thin films of $SmCo_5$. This approach provides an emerging experimental tool for high-resolution characterization of nanostructured magnetic systems with high spectroscopic sensitivity to local magnetic and structural heterogeneities. We proposed a simple model to understand the inclusions and their interaction with magnetic domain walls. With the promise of emerging ultrahigh brightness soft x-ray sources, our results point to similar studies with even higher resolution and spectral sensitivity, which will allow the full 3D spin structure near a magnetic nanostructure to be determined with few-nanometer resolution.

This work was supported by the Director, Office of Science, Office of Basic Energy Sciences, Materials Sciences and Engineering Division, of the U.S. Department of Energy under Contract No. DE-AC02-05-CH11231 within the "Non-Equilibrium Magnetic Materials" program. Work at the ALS was supported by the Director, Office of Science, Office of Basic Energy Sciences, Scientific User Facilities Division, of the U.S. Department of Energy under Contract No. DE-AC02-05-CH11231. J.L. and X.S. acknowledge partial supported by the U.S. Department of Energy, Office of Basic Energy Sciences, Division of Materials Science and Engineering, under Grant No. DE-FG02-11ER46831. S.M. is partially supported by the Center for Applied Mathematics for Energy Research Applications (CAMERA), which is a partnership between Basic Energy Sciences (BES) and Advanced Scientific Computing Research (ASCR) at the U.S. Department of Energy.

[1]S. D. Bader and S. S. P. Parkin, Annu. Rev. Condens. Matter Phys. **1**, 71 (2010).
[2]C. H. Marrows and B. J. Hickey, Philos. Trans. R. Soc. A **369**, 3027–3036 (2011).
[3]J. R. Skuza, C. Clavero, K. Yang, B. Wincheski, and R. A. Lukaszew, IEEE Trans. Magn. **46**, 1886 (2010).
[4]A. K. Sinha, M. N. Singh, A. Upadhyay, M. Satalkar, M. Shah, N. Ghodke, S. N. Kane, and L. K. Varga, Appl. Phys. A **118**, 291–299 (2015).
[5]N. Nagaosa and Y. Tokura, Nat. Nanotechnol. **8**, 899–911 (2013).
[6]R. Tomasello, E. Martinez, R. Zivieri, L. Torres, M. Carpentieri, and G. Finocchio, Sci. Rep. **4**, 6784 (2014).
[7]C. Phatak, Y. Liu, E. B. Gulsoy, D. Schmidt, E. Schubert, and A. Petford-Long, Nano Lett. **14**(2), 759 (2014).
[8]P. Fischer, IEEE Trans. Magn. **51**, 0800131 (2015).
[9]S. Eisebitt, J. Lüning, W. F. Schlotter, M. Lörgen, O. Hellwig, W. Eberhardt, and J. Stöhr, Nature **432**, 885–888 (2004).
[10]J. Miao, P. Charalambous, J. Kirz, and D. Sayre, Nature **400**, 342–344 (1999).
[11]J. Rodenburg, A. Hurst, A. Cullis, B. Dobson, F. Pfeiffer, O. Bunk, C. David, K. Jefimovs, and I. Johnson, Phys. Rev. Lett. **98**(3), 034801 (2007).
[12]M. Dierolf, A. Menzel, P. Thibault, P. Schneider, C. M. Kewish, R. Wepf, O. Bunk, and F. Pfeiffer, Nature **467**(7314), 436–439 (2010).
[13]D. A. Shapiro, Y. S. Yu, T. Tyliszczak, J. Cabana, R. Celestre, W. Chao, K. Kaznatcheev, A. L. D. Kilcoyne, F. Maia, S. Marchesini, Y. S. Meng, T. Warwick, L. L. Yang, and H. A. Padmore, Nat. Photonics **8**, 765–769 (2014).
[14]A. Tripathi, J. Mohanty, S. H. Dietze, O. G. Shpyrko, E. Shipton, E. E. Fullerton, S. S. Kim, and I. McNulty, Proc. Natl. Acad. Sci. U. S. A. **108**(33), 13393–13398 (2011).
[15]J. J. Turner, X. Huang, O. Krupin, K. A. Seu, D. Parks, S. Kevan, E. Lima, K. Kisslinger, I. McNulty, R. Gambino, S. Mangin, S. Roy, and P. Fischer, Phys. Rev. Lett. **107**, 033904 (2011).
[16]Y.-S. Yu, C. Kim, D. A. Shapiro, M. Farmand, D. Qian, T. Tyliszczak, A. L. D. Kilcoyne, R. Celestre, S. Marchesini, J. Joseph, P. Denes, T. Warwick, F. C. Strobridge, C. P. Grey, H. Padmore, Y. S. Meng, R. Kostecki, and J. Cabana, Nano Lett. **15**, 4282–4288 (2015).
[17]J. Kimling, F. Kronast, S. Martens, T. Boehnert, M. Martens, J. Herrero-Albillos, L. Tati-Bismaths, U. Merkt, K. Nielsch, and G. Meier, Phys. Rev. B **84**, 174406 (2011).
[18]R. Streubel, F. Kronast, P. Fischer, D. Parkinson, O. G. Schmidt, and D. Makarov, Nat. Commun. **6**, 7612 (2015).
[19]A. Hubert and R. Schäfer, *Magnetic Domains* (Springer, New York, 1998).
[20]V. Neu, J. Thomas, S. Fähler, B. Holzapfel, and L. Schultz, J. Magn. Magn. Mater. **242–245**, 1290–1293 (2002).
[21]V. Neu, U. Hannemann, S. Fähler, B. Holzapfel, and L. Schultz, J. Appl. Phys. **91**, 8180 (2002).
[22]J. Sayama, T. Asahi, K. Mizutani, and T. Osaka, J. Phys. D: Appl. Phys. **37**, L1–L4 (2004).
[23]J. B. Kortright and S. K. Kim, Phys. Rev. B **62**(18), 12216 (2000).
[24]A. Scherz, W. Schlotter, K. Chen, R. Rick, J. Stöhr, J. Lüning, I. McNulty, C. Günther, F. Radu, W. Eberhardt, O. Hellwig, and S. Eisebitt, Phys. Rev. B **76**(21), 214410 (2007).
[25]D. R. Luke, Inverse Probl. **21**(1), 37–50 (2005).
[26]S. Marchesini, A. A. Schirotzek, C. Yang, H. T. Wu, and F. Maia, Inverse Probl. **29**(11), 115009 (2013).
[27]M. Blume and D. Gibbs, Phys. Rev. B **37**(4), 1779–1789 (1988).
[28]M. van Heel and M. Schatz, J. Struct. Biol. **151**(3), 250–262 (2005).
[29]M. Howells, T. Beetz, H. N. Chapman, C. Cui, J. M. Holton, C. J. Jacobsen, J. Kirz, E. Lima, S. Marchesini, H. Miao, D. Sayre, D. A. Shapiro, J. C. H. Spence, and D. Starodub, J. Electron Spectrosc. Relat. Phenom. **170**(1–3), 4–12(2009).
[30]H. Kronmueller and R. Hertel, J. Magn. Magn. Mater. **215–216**, 11–17 (2000).
[31]D.-T. Ngo, Z. L. Meng, T. Tahmasebi, X. Yu, E. Thoeng, L. H. Yeo, A. Rusydi, G. C. Han, and K.-L. Teo, J. Magn. Magn. Mater. **350**, 42 (2014).
[32]See http://henke.lbl.gov/optical_constants/ for calculated X-ray absorption coefficients.
[33]M. J. Robertson, Ch. J. Agostino, A. T. N'Diaye, G. Chen, M.-Y. Im, and P. Fischer, J. Appl. Phys. **117**, 17D145 (2015).